A Scale-Aware Anticipated Potential Vorticity Method: On Variable-Resolution Meshes

QINGSHAN CHEN

Los Alamos National Laboratory, Los Alamos, New Mexico

MAX GUNZBURGER

The Florida State University, Tallahassee, Florida

TODD RINGLER

Los Alamos National Laboratory, Los Alamos, New Mexico

(Manuscript received 14 March 2012, in final form 30 May 2012)

ABSTRACT

A scale-aware formulation of the anticipated potential vorticity method (APVM), previously derived for quasi-uniform unstructured grids, is evaluated on multiresolution grids. Comparison is made to the original, nonscale-aware formulation of the APVM. Numerical experiments are performed using the shallow-water standard test case 5. The scale awareness of the new formulation is demonstrated by the following observations: (i) the range of optimal values for the single parameter of the new formulation is much less sensitive to grid resolution than that of the original formulation; (ii) within the optimal parameter range, the new formulation is able to maintain proper dissipation across scales and is thus able to produce better results in terms of errors in the potential enstrophy spectrum curves; and (iii) the new formulation is robust in that a single optimal parameter obtained for a specific grid can be safely used on other grids as well.

1. Introduction

In Chen et al. (2011) we developed a scale-aware formulation of the anticipated potential vorticity method (APVM; Sadourny and Basdevant 1985, also see below). Numerical experiments were conducted on quasi-uniform global spherical centroidal Voronoi tessellations (SCVT; Du et al. 1999, 2003) to demonstrate that the new formulation is able to self-adjust the level of dissipation as the resolution in the grid changes(i.e., it is scale aware). In this article, we explore the quality and robustness of the scale-aware APVM on multiresolution grids. The results in this article supplement those of Chen et al. (2011).

The APVM is a subgrid eddy closure scheme that is perfectly energy conserving and, at the same time, enstrophy dissipating. In the context of a shallow-water flow, the APVM modifies the momentum equation to give

$$\frac{\partial \mathbf{u}}{\partial t} + (q - D)\mathbf{k} \times h\mathbf{u} = -\nabla\left(\mathrm{gh} + \frac{1}{2}|\mathbf{u}|^2\right), \qquad (1)$$

where $\mathbf{u}$ and gh denote the velocity and geopotential fields, respectively; $q \equiv (\mathbf{k} \cdot \nabla \times \mathbf{u} + f)/h$ is the potential vorticity; D is a correction to the potential vorticity q; and $\mathbf{k}$ is the unit vector in the vertical direction. The modified system remains energy conserving, as the term $\mathbf{k} \times \mathbf{u}$ is perpendicular to the horizontal velocity component. The term D is chosen so that the modified system dissipates the potential enstrophy (i.e., the variance of the potential vorticity). In its simplest form, we have

$$D = \gamma \mathbf{u} \cdot \nabla q. \qquad (2)$$

It was proposed in Sadourny and Basdevant (1985) that γ should be a time-scale-selective parameter and thus should take the following form:

$$\gamma = \sigma dt, \qquad (3)$$

with dt denoting the time step and σ an independent parameter. In the scale-aware version of APVM

Corresponding author address: Qingshan Chen, Theoretical Division, Los Alamos National Laboratory, Los Alamos, NM 87545. E-mail: qchen@lanl.gov

DOI: 10.1175/MWR-D-12-00081.1

© 2012 American Meteorological Society

developed in Chen et al. (2011), γ takes the following form:

$$\gamma = \alpha \overline{\mathrm{ke}}^{-3/2} |\mathbf{u} \cdot \nabla q| \bar{h} \ell^3. \tag{4}$$

On the right-hand side of (4), $\overline{\mathrm{ke}}$ denotes the mean of the kinetic energy, $\bar{h}$ is the mean of the fluid thickness, ℓ is the local resolution, and α (the only free parameter) is independent of the characteristic scale of the flow.

The success in Chen et al. (2011) relies on the crucial fact that the grid-resolution-dependent factor in (4) enables the closure to adjust itself to the grid resolution changes. Specifically, it effects more dissipation as the grid coarsens, in a nonlinear fashion according to (4). The purpose of this article is to evaluate whether this new formulation of the APVM can act *appropriately* across different scales present on a multiresolution grid. The answer to this question cannot a priori be derived from the results on quasi-uniform grids, because the nonuniformity in grid resolution present in multiresolution grids may cause complications such as the deterioration of accuracy in the solutions and/or the hindering of waves from one resolution zone to another. Instead, we use a suite of multiresolution grids and numerically explore how well the APVM with the new formulation developed in Chen et al. (2011) acts across the wide range of scales present in these grids.

2. Numerical results and analysis

As with the evaluation of most closures, the measure of effectiveness is based on the ability of a low-resolution simulation with the closure to reproduce certain important aspects of a high-resolution, reference simulation. In the simulations below, we evaluate the closure based in its ability to reproduce the spectrum of the potential enstrophy (PE) obtained in the high-resolution simulation. Specifically, we define the "error" in an approximate solution as the mean distance between the PE spectrum curves, within the inertial range, of the approximate solution and the high-resolution reference solution. Let P (P_r) denote the spectral density function for the PE of the approximate (reference) solution. Then the error between the approximate and the reference solutions is defined as

$$d = \frac{1}{k_1 - k_0 + 1} \sum_{k=k_0}^{k_1} |\log \hat{P}(k) - \log \hat{P}_r(k)|, \tag{5}$$

where k denotes the spherical wavenumber, and k_0 and k_1 are the starting and ending wavenumbers, respectively, for the subrange. We should remark that our choice of error metric focuses on the power spectra of the potential enstrophy of the flow, and it neglects other aspects of the flow, such as wave phases, computational modes, etc. However, we believe that this choice of error metric is most relevant in the regime of turbulent flows.

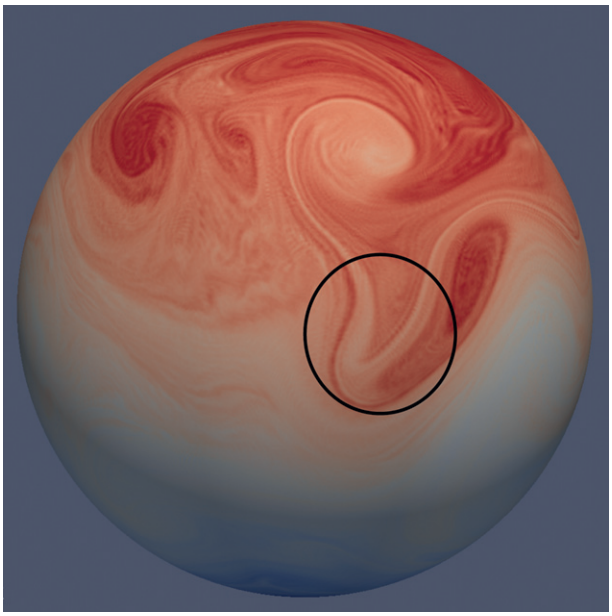

FIG. 1. The potential vorticity field on day 50, with values in the range from -3.2×10^{-8} m^{-1} s^{-1} to 3.2×10^{-8} m^{-1} s^{-1}. The location of the mountain is indicated by the circle. The axis of the globe is slightly tilted in order to better display the structure of the potential vorticity field on the Northern Hemisphere.

We conduct numerical experiments with the standard shallow-water test case 5, which involves an initially zonal flow impinging on a mountain topography. The model configurations are identical to those set forth in Williamson et al. (1992). We only remark that the topography is not a source or sink of potential vorticity, but instead acts as an inhomogeneity that leads to the breakdown of the nonlinearly balanced geostrophic zonal jet. There is no other external forces added, and therefore this is a slowly decaying turbulent flow. The reference solution is computed on an SCVT mesh with 655 362 cells ($dx \approx 30$ km), with the traditional ∇^4 dissipation of 10^9 m^4 s^{-1}. The shallow-water test case 5 evolves into turbulence in about 20–25 days. A snapshot of the potential vorticity field on day 50 is shown in Fig. 1. The spectrum of the potential enstrophy of the reference solution on day 150 is plotted in Fig. 2. An inertial range of width approximately one decade appears between wavenumbers 20 and 120, and approximately verifies the -1 power law for potential enstrophy spectra.

Approximate solutions are computed on variable-resolution grids refined in a region including the mountain topography. Specifically, the grids are refined in the

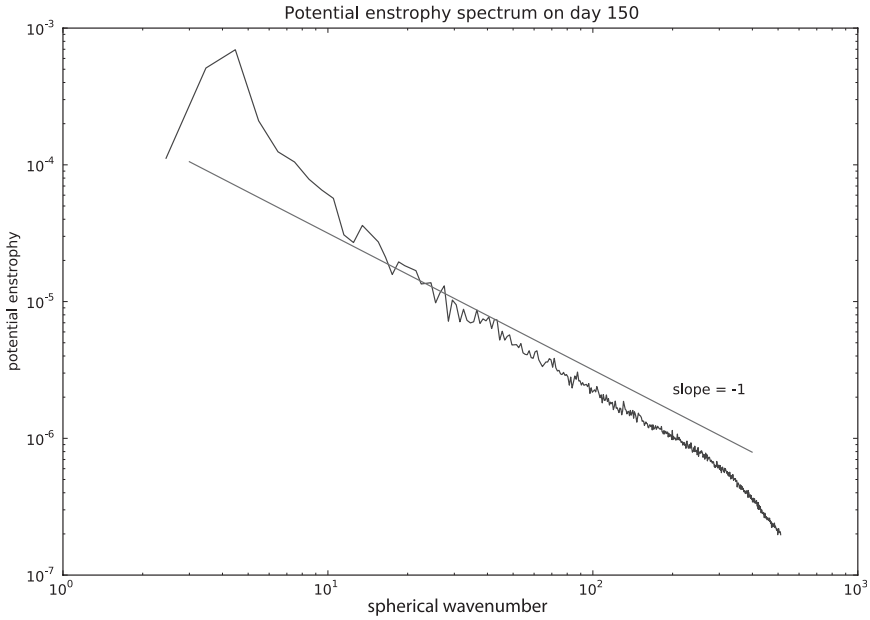

FIG. 2. The potential enstrophy spectrum on day 150 for the reference solution.

area 30° surrounding the center of the mountain topography, and smoothly coarsen outside this region. One set of grids has 40 962 cells, with the contrast ratio between the finest and coarsest grid resolutions ranging over {1, 2, 4, 8, 16}. Another set of grids has 163 842 cells, with the contrast ratio ranging over {1, 2}. More details and visual plots of these grids are available in Ringler et al. (2011). For our purpose, we list the resolutions of the fine and coarse regions of the aforementioned grids in Table 1. In what follows, these grids will be referred to as the 40 962-cell X1 grid, etc. We note that the midlatitude Rossby radius in the simulations is approximately 2000 km. The coarsest region in these meshes has a resolution of 592 km. Thus, in all simulations the Rossby radius is resolved. We also note that the finest region on these meshes has a resolution of 37 km, which is at the same level as the resolution (30 km) of the uniform high-resolution grid used for the reference solution.

The fine-resolution zones on the grids demand small time steps according to the Courant–Friedrichs–Lewy (CFL) criteria (Courant et al. 1967). The time step (see Table 1) used for each of the grid in our simulations is determined empirically so that stable solutions are achieved. In Chen et al. (2011), a strict invariance of the optimal parameter of the new formulation with respect to the time step size is demonstrated. The explanation is that the model incorporating the new APVM formulation consists of partial differential equations that are independent of the time step size and therefore the solutions of the model are independent of the time step size as well. This argument applies in the multiresolution setting as well, and therefore the invariance of the optimal parameter of the new formulation with respect to the time step size is assumed, and will not be explicitly addressed in this work. We note that, on each grid, the same time step is used for both the original and new APVM formulations. Hence, the following comparisons between the results of these two formulations are sensible.

On each of the grids mentioned above, a series of simulations with the original formulation (3) and the new formulation (4) of the APVM are conducted. The parameter σ of the original formulation assumes values starting from zero and increases by 0.002 for each simulation; the parameter α of the new formulation starts from zero, and increases by 0.0001 for each simulation. The increments in the sampling values of the parameters for both formulations are determined empirically so

TABLE 1. Grid information, time steps, and optimal parameters.

Grid	Resolutions	Time step (s)	Optimal parameters σ	Optimal parameters α
40 962-cell X1	(120, 120)	172.8	0.018	0.0018
40 962-cell X2	(65, 130)	172.8	0.018	0.0018
40 962-cell X4	(48, 190)	172.8	0.024	0.0024
40 962-cell X8	(39, 310)	86.4	0.074	0.0026
40 962-cell X16	(37, 592)	43.2	0.408	0.0033
163 842-cell X1	(60, 60)	172.8	0.004	0.0008
163 842-cell X2	(33, 65)	86.4	0.008	0.0012

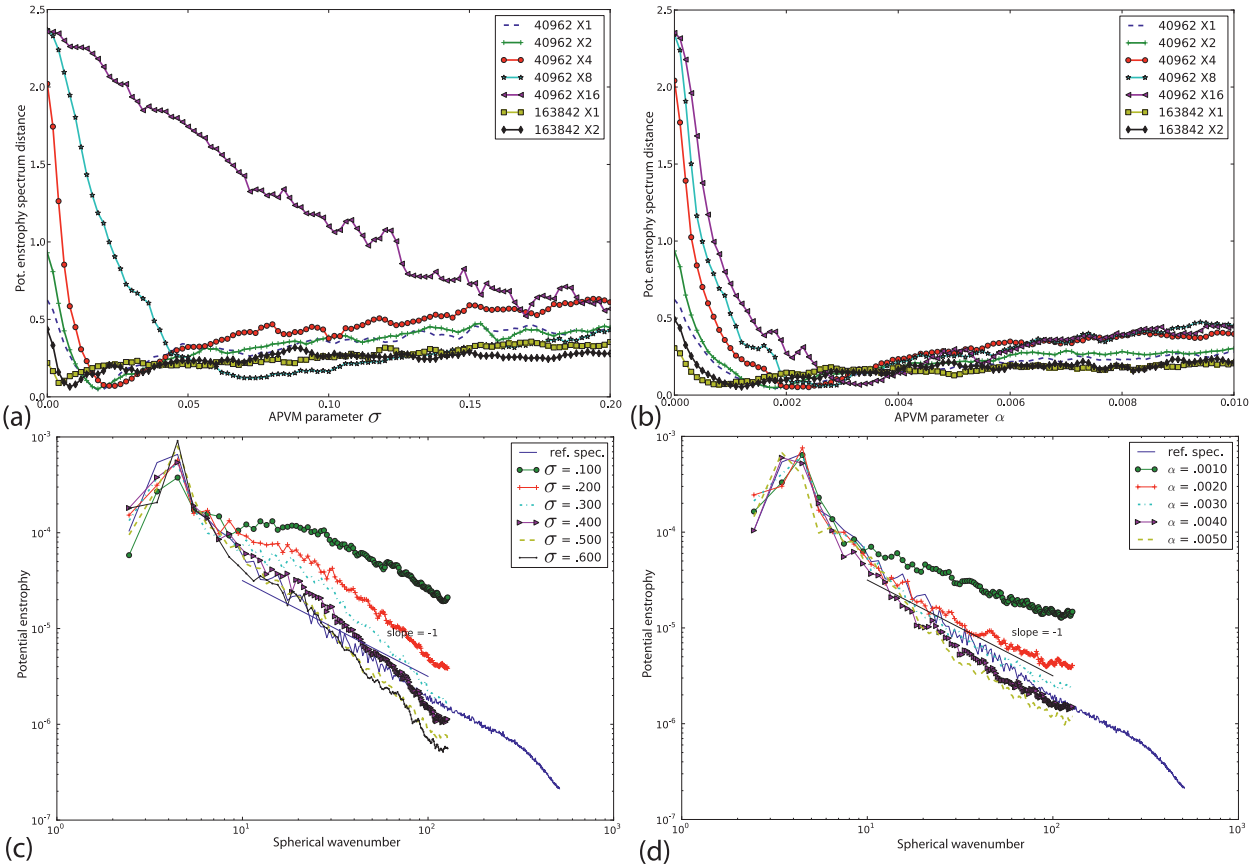

FIG. 3. Performance comparison for the original APVM and the new scale-aware APVM: (a) errors in the potential enstrophy spectra from simulations with the original APVM on a series of variable-resolution grids; (b) errors in the potential enstrophy spectra from simulations with the scale-aware APVM on a series of variable-resolution grids; (c) the potential enstrophy spectrum curves with the original APVM with σ = 0.1, 0.2, 0.3, 0.4, 0.5, 0.6, on the 40 962-cell X16 variable-resolution grid; (d) the potential enstrophy spectrum curves with the scale-aware APVM with α = 0.0010, 0.0020, 0.0030, 0.0040, 0.0050, on the 40 962-cell X16 variable-resolution grid.

that, with around ~100 simulations, a good sample is obtained in most cases except for the extreme case of the original APVM on the 40 962 X16 grid, which requires 300 simulations.

For each simulation, the error in the approximate solution compared to the high-resolution reference solution is computed using (5). The errors for the original APVM formulation, on all the aforementioned grids, are plotted against the original APVM parameter σ in Fig. 3a. The error curve for the 40 962 X16 grid is truncated on this plot. The high contrast ratio between the fine and coarse resolutions on this grid demands a much wider parameter interval in order to reveal the optimal parameter. The whole error curve on this grid, obtained on an interval of [0, 0.60], continues to decrease beyond σ = 0.20, flattens and reaches its minimum at σ = 0.408, and then rises up again. The errors for the new APVM formulation, on all the aforementioned grids, are plotted in Fig. 3b against the new APVM parameter α. The optimal parameters for the new and original formulations of the APVM, on each of the grids used for this study, are listed in Table 1. It is seen that the optimal parameter for the original formulation ranges from 0.004 to 0.408, with a factor of 100 change! The optimal parameter for the new formulation ranges from 0.0008 to 0.0033, with a factor of 4 change. On variable-resolution grids, it is not possible to correlate the optimal parameter to the grid resolutions because of the presence of a wide range of grid scales. However, the fact that the range for the values of the optimal parameter of the new formulation is much narrower than that for the original formulation is the first indicator that the new APVM formulation is able to act appropriately across scales (i.e., it is scale aware).

The scale-aware property of the new formulation is also demonstrated by the fact that, on all the grids used

for this study, the new formulation produces minima that are at least as low as those produced by the original formulation. In certain situations (e.g., on the 40 962-cell X8 and the 40 962-cell X16 grids), it actually produces lower minima, thanks to its ability to act appropriately across the vast range of scales present on these grids.

The 40 962-cell X16 grid causes a surge in the value of the optimal parameter for the original formulation (Table 1). A detailed look at the spectrum curves produced with various parameter values on the 40 962-cell grid reveals why this happens, and also demonstrates more clearly the strength of the scale-aware feature of the new formulation. In Fig. 3c, we plot the PE spectrum curves with σ = 0.100, 0.200, 0.300, 0.400, 0.500, and 0.600 for the original formulation of the APVM. At σ = 0.100, which is already larger than the optimal parameter of the original formulation on any other grid, the spectrum curve stays way above the reference spectrum curve. Its straying behavior near wavenumber 10 reveals that the large-scale motions of the flow are corrupted, apparently due to the lack of dissipation in the coarse region of the mesh. Larger values are needed for the parameter σ to ensure proper dissipation in the coarse region. When the parameter has been raised to levels (σ = 0.400, 0.500, 0.600) for which the spectrum curves near wavenumber 10 match the reference spectrum curve reasonably well, the curves at high wavenumbers suffer from overdissipation in the fine regions. It is clear that the conflicting needs of dissipation in the coarse and fine regions on the mesh make it very challenging to bring the PE spectrum curve of the approximate solution evenly close to that of the reference solution. In Fig. 3d, we plot the PE spectrum curves produced with α = 0.0010, 0.0020, 0.0030, 0.0040, and 0.0050 for the APVM in the new formulation. Starting from α = 0.0010, as the parameter increases, the spectrum curve comes down at both low (10) and high (100) wavenumbers, demonstrating that the new formulation maintains control at both the low and high wavenumbers equally well. It can be seen that, at α = 0.0030, the spectrum curve of the approximate solution is close to the reference spectrum curve across the inertial range. As Table 1 shows, the optimal value for α on the 40 962-cell X16 grid is 0.0033.

As the foregoing results and analysis have shown, the scale-aware APVM formulation is able to act appropriately across grid scales, and produces better results compared to the original formulation, in situations where a vast range of scales are present. The results have also shown that the parameter of the new formulation is not strictly scale invariant, because it varies, albeit with a relatively small factor of change. Hence, it is crucial to assess the robustness or the insensitivity of the scale-aware APVM with respect to the parameter values near the numerically identified optimal values. To this end, we pick α = 0.0020, a representative value in the range [0.0011, 0.0032] found before for the optimal parameter of the new formulation, and plot, in Fig. 4, the spectrum curves produced with this value of the parameter, on all the grids used for this study. We see that the curves from the 40 962-cell X1, 40 962-cell X2, 40 962-cell X4, 163 842-cell X1, and 163 842-cell X2 grids match very well with the reference spectrum curve. The 40 962-cell X8 and 40 962-cell X16 grids are known to be challenging for numerical simulations due to the presence of a vast range of scales. Even so, the spectrum curves produced with the representative parameter value on these two grids stay reasonably close to the reference spectrum curve. To conclude this section, we note that the chosen optimal parameter α = 0.0020 here is consistent with the optimal interval found in Chen et al. (2011) for the new APVM formulation on quasi-uniform grids.

3. Conclusions

In this work, we numerically evaluate the scale-aware property of a new formulation of the APVM on multiresolution grids. Numerical simulations are conducted on a sample set of variable-resolution SCVT grids. Comparison is made between the new formulation and the original formulation, which has been used in earlier work. The scale-aware property of the new formulation is demonstrated by the fact that (i) the range for the optimal parameter of the new formulation is much narrower than that for the original formulation; (ii) on grids that are challenging for numerical simulations due to the high contrast ratios between fine and coarse resolutions, the new APVM formulation produces lower minima at the identified optimal parameters; and (iii) the APVM closure with the new formulation is less sensitive to the parameter near the numerically identified optimal values.

Our success with the APVM demonstrates that this closure is a viable option in simulating geophysical flows. Though admittedly, for more realistic flows, some simplifying assumptions that are valid in the case of shallow-water flows will have to be carefully reevaluated. Below we remark on a few key issues that need to be addressed when generalizing this closure to more realistic flows.

The closure presented in this work includes the assumption of small variations in fluid thickness; namely, we assume that variations in the fluid thickness h are small compared to the mean fluid thickness $\bar{h}$. For a broad class of shallow-water systems where this closure might be utilized, this will, in general, be a valid assumption. However, as we apply the closure to more

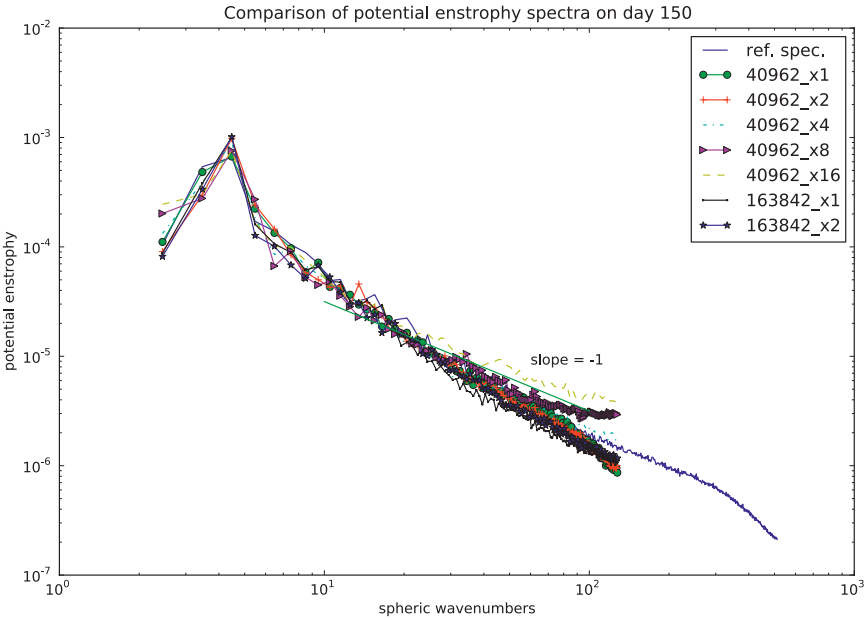

FIG. 4. Plots of the potential enstrophy spectrum on 40 962-cell X2, 40 962-cell X4, 40 962 X8, 40 962 X16, 163 842 X1, and 163 842 X2 variable-resolution grids. The parameter α is taken as the mean (0.0020 for this plot) of the possible range [0.0011, 0.0032].

realistic systems, such as the isopycnal model of the ocean circulation [see, e.g., Ringler and Gent (2010, manuscript submitted to *Ocean Modell.*)], this assumption will have to be revisited.

The scale-aware formulation presented in Chen et al. (2011) and the current work is derived based on another crucial assumption, namely the isotropy of the flow. Even though this assumption is approximately true for many cases, it is conceivable that, in order to faithfully represent a realistic geophysical flow, nonisotropic features of the flow will need to be taken into account. For example, the wave–turbulence interactions (see, e.g., Pedlosky 1987; Rhines 1975) have profound influence on the long-term behavior of the global oceanic and atmospheric circulations, and should be considered in designing subgrid closures.

Finally, this scale-aware formulation of APVM is most appropriate for geophysical flows with a potential enstrophy inertial range leading into the grid scale. Such a potential enstrophy inertial range appears to be present in mesoscale ocean modeling systems between the scale of mesoscale eddies (~200 km) and the model grid scale (~10 km; Fox-Kemper and Menemenlis 2008). Therefore, the next step will be to implement this closure within a global ocean modeling system that resolves mesoscale eddies. In particular, our intention is to use an ocean model constructed from the Model for Prediction Across Scales (MPAS) framework (Ringler et al. 2011) where the use of variable-resolution meshes requires parameterizations to act appropriately across a wide range of grid scales.

Acknowledgments. This work was supported by the Regional and Global Climate Modeling Program of the Office of Biological and Environmental Research within the U.S. Department of Energy's Office of Science. M. Gunzburger was supported by the U.S. Department of Energy Grant DE-SC0002624.

REFERENCES

Chen, Q., M. Gunzburger, and T. Ringler, 2011: A scale-invariant formulation of the anticipated potential vorticity method. *Mon. Wea. Rev.,* **139,** 2614–2629.

Courant, R., K. Friedrichs, and H. Lewy, 1967: On the partial difference equations of mathematical physics. *IBM J. Res. Develop.,* **11,** 215–234.

Du, Q., V. Faber, and M. Gunzburger, 1999: Centroidal Voronoi tessellations: Applications and algorithms. *SIAM Rev.,* **41** (4), 637–676.

——, M. Gunzburger, and L. Ju, 2003: Constrained centroidal Voronoi tessellations for surfaces. *SIAM J. Sci. Comput.,* **24** (5), 1488–1506.

Fox-Kemper, B., and D. Menemenlis, 2008: Can large eddy simulation techniques improve mesoscale-rich ocean models? *Ocean Modeling in an Eddying Regime, Geophys. Monogr.,* Vol. 177, Amer. Geophys. Union, 319–338.

Pedlosky, J., 1987: *Geophysical Fluid Dynamics*. 2nd ed. Springer, xiv+710 pp.

Rhines, P. B., 1975: Waves and turbulence on a beta-plane. *J. Fluid Mech.,* **69** (3), 417–443.

Ringler, T., D. Jacobsen, M. Gunzburger, L. Ju, M. Duda, and W. Skamarock, 2011: Exploring a multi-resolution modeling approach within the shallow-water equations. *Mon. Wea. Rev.,* **139,** 3348–3368.

Sadourny, R., and C. Basdevant, 1985: Parameterization of subgrid-scale barotropic and baroclinic eddies in quasi-geostrophic models: Anticipated potential vorticity method. *J. Atmos. Sci.,* **42,** 1353–1363.

Williamson, D. L., J. B. Drake, J. J. Hack, R. Jakob, and P. N. Swarztrauber, 1992: A standard test set for numerical approximations to the shallow water equations in spherical geometry. *J. Comput. Phys.,* **102,** 211–224.